Catalysis Letters (2020) 150:1434–1444
https://doi.org/10.1007/s10562-019-03034-9

Stability of Iron-Molybdate Catalysts for Selective Oxidation of Methanol to Formaldehyde: Influence of Preparation Method

Kristian Viegaard Raun[1] · Lars Fahl Lundegaard[2] · Pablo Beato[2] · Charlotte Clausen Appel[2] · Kenneth Nielsen[3] · Max Thorhauge[2] · Max Schumann[1] · Anker Degn Jensen[1] · Jan-Dierk Grunwaldt[4] · Martin Høj[1]

Received: 20 September 2019 / Accepted: 4 November 2019 / Published online: 15 November 2019

Abstract

Iron molybdate/molybdenum oxide catalysts with varying content of Mo (Mo/Fe = 1.6 and 2.0) were synthesized by a mild hydrothermal method and structurally characterized by XRD, XPS, Raman spectroscopy, SEM–EDX, BET and ICP-OES. The stability of the prepared catalysts in selective oxidation of methanol to formaldehyde was investigated by catalytic activity measurements for up to 100 h on stream in a laboratory fixed-bed reactor (5% MeOH, 10% O_2 in N_2, temp. = 380–407 °C). Excess MoO_3 present in the catalyst volatilized under reaction conditions, which lead to an initial loss of activity. Interestingly, the structure of the excess MoO_3 significantly affected the stability of the catalyst. By using low temperature hydrothermal synthesis, catalysts with the thermodynamically metastable hexagonal h-MoO_3 phase was synthesized, which yielded relatively large crystals (2–10 µm), with correspondingly low surface area to volume ratio. The rate of volatilization of MoO_3 from these crystals was comparatively low, which stabilized the catalysts. It was furthermore shown that heat-treatment of a spent catalyst, subject to significant depletion of MoO_3, reactivated the catalyst, likely due to migration of Mo from the bulk of the iron molybdate crystals to the surface region.

Graphical Abstract

$Fe_2(MoO_4)_3/MoO_3$ catalysts for selective oxidation of methanol were synthesized by hydrothermal synthesis forming large hexagonal-MoO_3 crystals. Significantly lower rate of catalyst deactivation due to volatilization of MoO_3 under reaction conditions was observed for the large h-MoO_3 compared to smaller crystals of thermodynamically stable α-MoO_3.

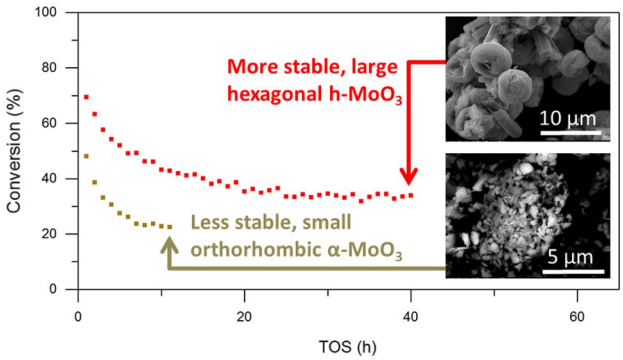

Keywords Formox · Formaldehyde · Iron molybdate · Hexagonal MoO_3 · Catalyst deactivation

1 Introduction

Formaldehyde (CH_2O) is one of the most important industrial intermediate chemicals, with a wide range of applications in chemical processes due to its high reactivity. In

Electronic supplementary material The online version of this article (https://doi.org/10.1007/s10562-019-03034-9) contains supplementary material, which is available to authorized users.

✉ Martin Høj
mh@kt.dtu.dk

Extended author information available on the last page of the article

2017 approximately 52 million tons of formalin (37 wt% aqueous CH_2O) were produced, and with an estimated annual growth rate of over 5%, the demand is increasing [1]. Formaldehyde is used industrially to produce a wide range of products, where formaldehyde resins account for approximately 75% of the consumption [2].

Formaldehyde is mainly produced from methanol by selective oxidation [3] according to reaction (1):

$$CH_3OH + 1/2O_2 \rightarrow CH_2O + H_2O \quad \Delta H = -156\,\text{kJ/mol} \tag{1}$$

The reaction is catalyzed by an iron molybdate/molybdenum oxide catalyst in a multi-tube, fixed bed reactor with excess of oxygen (~ 10% MeOH, ~ 5% H_2O, 10% O_2 in N_2) under slight over pressure (~ 0.5 barg) [4]. The process is known as the Formox process [5]. The formaldehyde yield is between 88 and 92% with complete methanol conversion in a single pass. When the feed gas is introduced to the catalytic bed it is quickly heated due to the highly exothermic reaction (1), typically reaching 350–400 °C in the hot spot of the reactor [6]. The presence of water vapor, and relatively low concentration of oxygen in the feed gas is obtained by mixing recycle gas to the feed stream of methanol and air, which keeps the risk of explosion low [5]. The temperature should be kept below 400 °C to limit side reactions, such as formation of CO/CO_2 and to assure the stability of the catalyst [7].

Söderhjelm et al. [8] studied the synergy between the MoO_3 and $Fe_2(MoO_4)_3$ phases in the iron molybdate catalyst. They tested catalysts with different Mo/Fe ratios (Pure Fe_2O_3, 0.2, 0.5, 1, 1.5, 2.2 and pure MoO_3). They achieved the highest selectivity and activity for the catalyst with a Mo/Fe ratio of 2.2. This catalyst consisted of a bulk phase of $Fe_2(MoO_4)_3$, bulk MoO_3 and a surface layer phase of MoO_x. They concluded that there is a synergy effect between the active surface layer (MoO_x) and the underlying sublayers ($Fe_2(MoO_4)_3$) of the catalyst. The catalyst was as selective towards formaldehyde as pure MoO_3, which is less active [9–11], and almost as active as pure $Fe_2(MoO_4)_3$, which is less selective. The synergy between the two phases in the iron molybdate catalyst thus yields a catalyst with both relatively high selectivity and activity. These observations have been confirmed by other researchers [12–14].

A major challenge for the Formox process is that molybdenum forms volatile species with methanol under reaction conditions, which leave behind an Mo depleted and less active catalyst [15–17]. Initially, the excess MoO_3 volatilizes followed by volatilization of Mo from the ferric molybdate phase ($Fe_2(MoO_4)_3$), present in the fresh catalyst, under formation of the reduced ferrous molybdate ($FeMoO_4$). Reduction of the ferric molybdate mainly takes place at temperatures above 300 °C [6]. At substantial molybdenum loss, Fe_2O_3 can be formed. Due to segregation of molybdenum in ferric molybdate, this phase tends to have an over stoichiometric Mo/Fe ratio on the surface [18].

Popov et al. [15] studied the deactivation and Mo volatilization from an iron molybdate/molybdenum oxide catalyst system (Mo/Fe = 1.5–2.5) under varying conditions of MeOH (up to 11.5 vol%) in air. They used a fixed bed reactor with a circulation loop and a trap for volatile Mo compounds placed downstream in the setup. They concluded that the rate of Mo volatilization is mainly affected by the methanol concentration and suggested the formation of the volatile compounds such as $MoO_2(OCH_3)_2$, $MoO_2(OH)(OCH_3)$, $MoO_2(OCH_3)$ and $MoO_2(OH)$. They observed that the volatile Mo species condensed as a blue film on the reactor tube inner surface at the reactor outlet and concluded that loss of Mo from the catalyst surface is the main reason for deactivation of the catalyst.

It is well known that volatile Mo compounds are transported through the industrial reactor and deposit downstream in the catalytic bed, which leads to an increased pressure drop [17]. The life time of the industrial process is only 1 to 2 years due to either loss of selectivity or development of a too high pressure drop, which is a major unsolved issue [16].

Commercial iron molybdate catalysts are usually prepared by co-precipitation followed by calcination [19], yielding an over-stoichiometric iron molybdate catalyst containing the $Fe_2(MoO_4)_3$ phase and the thermodynamically stable α-MoO_3 phase. However, MoO_3 can form several crystal structures depending on preparation conditions. α-MoO_3 has an orthorhombic structure (β = 90°) consisting of layers built from edge-sharing, distorted MoO_6 octahedra and possesses terminal Mo=O bonds [20]. Molybdenum trioxide can form two other metastable structures: β-MoO_3, and hexagonal h-MoO_3, which are typically synthesized at low temperature. β-MoO_3 has a monoclinic structure, built by three-dimensional corner-sharing octahedral MoO_6 units. As oxygen atoms are multiply bonded to Mo atoms, only the surface positioned octahedral units possesses unshared corner oxygen atoms forming terminal Mo=O bonds. β-MoO_3 transforms to α-MoO_3 at around 450 °C [21]. h-MoO_3 is a metastable hexagonal structure, that has been observed to transform to α-MoO_3 at 400 to 419 °C [22, 23].

We have studied the ageing of an iron molybdate/molybdenum oxide catalyst (Mo/Fe = 2) under reaction conditions (25 mg catalyst, 5% MeOH, 10% O_2 in N_2, temp. = 384–416 °C, W/F = 1.2 $g_{cat}h\ mol^{-1}_{MeOH}$) for an extended period of up to 600 h [24]. Excess α-MoO_3 was shown to volatilize and leave the catalyst during the first 10 h on stream, leading to an initial decrease in activity of approximately 50%. From 10 to 600 h on stream vaporization of molybdenum from the remaining iron molybdate phase ($Fe_2(MoO_4)_3$, Mo/Fe = 1.5) lead to formation of iron rich phases ($FeMoO_4$ and Fe_2O_3, Mo/Fe < 1.5) and simultaneously an increase in catalytic activity above the initial

activity. Even at high degrees of molybdenum loss, the formaldehyde selectivity remained above 92%, which was explained by a surface layer of MoO_x on the catalyst at all times due to segregation of Mo from the iron molybdate phase. After 600 h on stream, formation of β-MoO_3 was observed, indicating that this molybdenum oxide phase is stable to some extent under reaction conditions. The initial loss of the α-MoO_3 was additionally confirmed and studied using operando X-ray diffraction (XRD), X-ray absorption spectroscopy (XAS) and Raman spectroscopy [25].

This work presents further studies of the iron molybdate catalyst system, its stability and ways to increase the stability. We have synthesized catalysts with varying Mo/Fe ratios (1.6 and 2.0) to show the effect of adding excess MoO_3 to counter the effect of Mo volatilization. Furthermore, we show, for the first time, the stabilizing effect of synthesizing a catalyst (Mo/Fe = 2) with large crystals of h-MoO_3 present as the excess MoO_3 phase. The stabilizing effect may be utilized to extend the catalyst lifetime, which is only 1 to 2 years nowadays and the major technical issue in the industry. Finally, we show that Mo depleted catalysts can be reactivated by heat treatment.

2 Experimental

2.1 Catalyst Preparation

The iron molybdate catalysts were prepared by hydrothermal synthesis similar to the procedure reported by Beale et al. [26] and previously used by the authors [24]. Iron nitrate nonahydrate [$Fe(NO_3)\cdot 9H_2O$—Sigma Aldrich > 98% purity] and ammonium heptamolybdate tetrahydrate [$(NH_4)_4Mo_7O_{24}\cdot 7H_2O$—Sigma Aldrich > 99% purity] were dissolved separately in 150 mL of demineralized water each. The ammonium heptamolybdate solution was dropwise added to the iron nitrate solution under vigorous stirring. Some precipitation occurred immediately after mixing. The mixture was loaded in a 400 mL Teflon-lined autoclave (Berghof) with a magnetic stirrer and the pH was measured (1.7–2.2). The autoclave was sealed, heated to 180 °C and kept at this temperature for hydrothermal treatment of the mixture for 12 h. The solid product was filtered, washed with demineralized water and dried at 60 °C overnight yielding a yellow/green powder (yield ≈ 90%).

2.2 Catalytic Activity Measurements

The synthesized catalyst powders were pressed into pellets, crushed and sieved to 150–250 µm sieve fractions. A bed containing 25 mg catalyst and 170 mg SiC (150–300 µm sieve fraction) was placed between two plugs of quartz wool in a U-tube reactor (ID = 4 mm). The reactor was placed in an oven. The feed gas consisted of 10 vol% O_2 and ~ 5 vol% MeOH in N_2, which was fed at a flowrate of ~ 157.5 mL/min (1 bar, 273.15 K). N_2 and O_2 were introduced by mass flow controllers (Brooks) and bubbled through a flask containing MeOH (≥ 99.9%, Sigma-Aldrich). The gas was saturated with MeOH and the concentration was controlled by cooling the bubble-flask in a cooling bath to 5 °C. To determine the conversion and selectivity the gas composition was measured at the outlet of the reactor by a gas chromatograph (GC) (Thermo Scientific, Trace GC Ultra). The MeOH and DME concentrations were measured using an FID-detector and the CH_2O, H_2O, CO, CO_2, O_2 and N_2 concentrations were measured using a TCD-detector. The measured concentrations were corrected for expansion of the gas due to reaction using the N_2 signal as internal standard [27]. Furthermore, the reactor inlet and outlet pressures were measured, and a thermocouple was placed inside the reactor touching the exit of the catalyst bed to measure the bed temperature. Before each experiment, the catalyst bed was thermally treated at 400 °C in air for 2 h and the conversion was subsequently measured at increasing temperatures (oven temp. = 250, 300, 340 and 375 °C) under reaction conditions to obtain the first order reaction rate constant as a function of temperature. Due to fast changes in the catalytic activity under reaction conditions, the oven temperature was increased without MeOH in the feed (10% O_2 in N_2). When the oven temperature stabilized at the new set point, MeOH was introduced for 5 min followed by a gas composition measurement. The measurement at 375 °C was also the first measurement of the following prolonged measurement of catalyst deactivation. The changes in the catalytic activity prior to the deactivation experiment were small due to the short exposure time and moderate temperature. The deactivation experiments ran for 100 h (oven temp. = 375 °C, 1 GC-measurement per hour). After the 100 h test, the catalyst was heat treated at an oven temperature of 400 °C for 2 h under 10% O_2 and 90% N_2, followed by a 4 h run under the previous reaction conditions. This procedure was repeated with heat treatment at 500 °C for 2 h. Finally, the catalyst was cooled to room temperature in the reaction gas mixture to maintain the catalyst state.

2.2.1 GC-Calibration

Both GC detectors (FID and TCD) were calibrated using gas mixtures with known concentrations, except for formaldehyde due to its ability to polymerize at room temperature. The TCD detector was calibrated for formaldehyde using Lennard–Jones parameters to calculate the viscosity and thermal conductivity for formaldehyde and reference species (N_2, O_2, MeOH and CH_4). A linear trend between the TCD detector response factor and the thermal conductivity for the respective reference species was seen. The response factor of formaldehyde could be estimated by assuming a

linear trend of the reference species [28–30]. The response factor of formaldehyde was similar to the response factors for N_2, O_2 and MeOH, which have similar molar masses.

2.2.2 Calculation of Selectivity and Conversion

The conversion of methanol (X) and selectivity to formaldehyde (S) was calculated according to Eqs. (2) and (3):

$$X = \left(1 - \frac{P_{MeOH}}{P_{MeOH} + P_{CH_2O} + 2P_{DME} + P_{CO} + P_{CO_2}}\right) \times 100\% \quad (2)$$

$$S = \frac{P_{CH_2O}}{P_{MeOH} + P_{CH_2O} + 2P_{DME} + P_{CO} + P_{CO_2}} * 100\% \quad (3)$$

The carbon balance with respect to all measured compounds closed within 7% (see ESI Figs. S1 to S4).

Beside oxidation of formaldehyde into CO and CO_2, DME is industrially observed as a side product. The formation of DME is a reversible reaction between two methanol molecules according to (4). At higher conversion levels DME will mainly be converted to formaldehyde yielding high overall selectivity.

$$2CH_3OH \rightleftarrows (CH_3)_2O + H_2O \quad (4)$$

2.3 Catalyst Characterization

2.3.1 X-ray Diffraction

XRD data were collected using a PanAlytical Empyrean diffractometer equipped with focusing mirrors for Cu K_α radiation ($\lambda = 1.541$ Å) and a capillary spinner. A Ni beta filter, a pair of 0.04 rad soller slits and a beam stop were used. Samples were measured in sealed capillaries. Rietveld refinement was performed using the TOPAS software [31] with reference structures for $Fe_2(MoO_4)_3$ [ICSD 80449], $FeMoO_4$ [ICSD 43013], α-MoO_3 [ICSD 152313], h-MoO_3 [ICSD 80291] and Fe_2O_3 [ICSD 15840]. Atomic positions and stoichiometry were fixed, while lattice parameters, average crystallite size and scale factors were refined.

2.3.2 Raman Spectroscopy

Raman spectra were recorded with a Horiba LabRAM microscope, using 633 nm excitation. The samples were sealed in glass capillaries in order to avoid re-oxidation in air during measurements. A 50× long distance objective (Olympus) was used to focus the laser beam, with a measured power of 1 mW on the sample. Reference spectra for all relevant phases are shown in the Electronic Supplementary Information (ESI) Fig. S5.

2.3.3 Electron Microscopy (SEM–EDX)

The particles were dispersed on double sided carbon tape on an aluminum stub and the samples were coated with an electron conductive layer of carbon prior to investigation. Scanning Electron Microscopy (SEM) images were acquired in an Environmental SEM, XL30 FEG, at 15 kV using the backscattered electron signal.

EDX analyses in the SEM microscope were acquired without standards at 15 kV with an EDAX liquid nitrogen cooled Si(Li) detector.

2.3.4 Surface Analysis by X-ray Photoelectron Spectroscopy (XPS)

XPS was performed with a Theta Probe system from Thermo Fisher Scientific. The system utilizes monochromatized Al K_α X-rays with an energy of 1486.7 eV as the source and the spot size was set to 400 µm (diameter). A hemispherical analyzer was used for data acquisition and the data were analyzed with the Avantage software package version 5.979 from Thermo Fisher.

2.3.5 Bulk Analysis by ICP-OES

The catalyst samples were decomposed by fusion with potassium pyrosulphate, and dissolved by adding concentrated hydrochloric acid. The element concentration was determined using a Perkin Elmer model Optima 3000 ICP/OES analyser. The corresponding Mo/Fe ratio of the measured samples are shown in Table 1.

2.3.6 BET-Surface Area

The specific surface area (SSA) was measured on the fresh catalysts, after degassing at 350 °C under vacuum, by nitrogen adsorption at its boiling point using multipoint BET theory with four points in the $p/p_0 = 0.15$ to 0.3 range (Quantachrome NOVAtouch LX2). The corresponding surface areas of the measured samples are shown in Table 1.

Table 1 Atomic Mo/Fe bulk ratio according to ICP-OES and specific surface area (SSA) according to BET

Sample	Mo/Fe bulk ratio	SSA [m^2/g]
FeMo_1.6h	1.63	6.8
FeMo_2.0h	1.98	7.8
FeMo_2.0α [24]	2.01	4.7

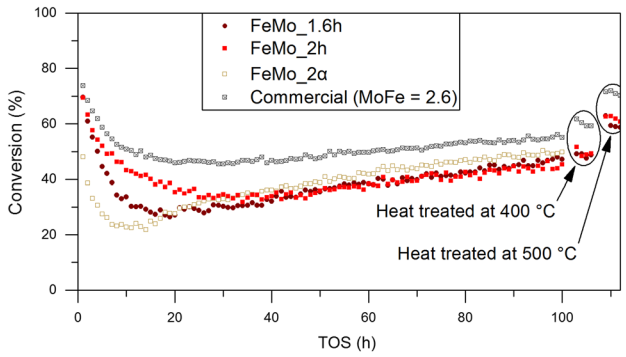

Fig. 1 MeOH conversion as function of time on stream for all samples. FeMo_2.0h, FeMo_1.6h and the commercial sample were reactivated at 400 °C after 100 h, and again at 500 °C after 106 h. Operating conditions: 25 mg catalyst mixed with 170 mg SiC, ~157.5 NmL min^{-1} gas, feed composition: 10% O_2, ~5% MeOH in N_2. During reactivation: 10% O_2 in N_2. Oven temperature: 375 °C yielding a bed temperature of 380–407 °C Ambient pressure: FeMo_2.0α is adapted from [24]

Table 2 Apparent activation energy for all catalyst samples

Sample	Activation energy (kJ/mol)
FeMo_1.6h	59
FeMo_2.0h	51
FeMo_2.0α	54
Commercial	63

2.4 Catalyst Samples

The catalyst samples in this study are named by their Mo/Fe ratio and the structure of the initially present MoO_3 phase. For example, the sample with a Mo/Fe ratio of 2.0 and an initial hexagonal structure of the MoO_3 phase (h-MoO_3) is named FeMo_2.0h.

3 Results and Discussion

3.1 Catalytic Activity Measurements

Figure 1 shows the methanol conversion as function of time on stream for the three FeMo catalysts investigated in this study and a commercial reference catalyst (Mo/Fe = 2.6). The combined selectivity towards formaldehyde and the reversible side product DME was above 97% and the bed temperature was 380–407 °C throughout all the experiments. The activation energy (Table 2) of the reaction on the catalysts was determined prior to each experiment by measuring the methanol conversion at increasing temperature and assuming a first order reaction in methanol, to calculate the rate constant as described in Ref. 24. Based on the rate constants, the activation energy is obtained from corresponding the Arrhenius plot, see ESI Fig. S6. The measured apparent activation energies in this study were similar to activation energies (61 and 57 kJ/mol) reported in the literature [32, 33]. All activity measurements including selectivities to all measured products are shown in the ESI Figs. S1–S4.

For all samples, the conversion decreased to approximately half of the initial conversion over a period of 10 to 40 h, correlated with volatilization of all excess MoO_3 [24, 25]. The sample with less MoO_3 (FeMo_1.6h) and the sample with α-MoO_3 (FeMo_2.0α) lost activity faster than the sample with h-MoO_3 (FeMo_2.0h) and the commercial sample with more α-MoO_3 (Mo/Fe = 2.6). The initial decrease in conversion was followed by a slow increase throughout the 100 h on stream, as observed previously [24]. It should be noted that during the slow increase in activity, an increasing formation of CO was measurable (see ESI Figs. S1 to S4), which would lead to a decreased yield in an industrial plant operated at complete conversion of methanol. Furthermore, throughout the activity measurements the selectivity to DME was highest when the conversion was relatively low (see ESI Figs. S1 to S4). This is due to the reversible formation of DME from methanol. At higher conversion levels of methanol, DME is converted back to methanol, which decreases its overall selectivity.

FeMo_1.6h, FeMo_2.0h and the commercial sample were heat treated after 100 h on stream, as described in the experimental section (Sect. 2.2). By heat treating the catalyst at 400 °C under an aerobic feed flow, the samples were partly reactivated, increasing the conversion by about 2–6% points. Further reactivation by heat treatment at 500 °C significantly increased the conversion by about 17% points relative to after the first 100 h on stream.

3.2 Catalyst Characterization

The catalysts were characterized after synthesis and after the catalytic activity and deactivation measurements. An overview of the characterizations (XRD, Raman spectroscopy and XPS) is shown in Table 3.

In our previous work [24], a catalyst with Mo/Fe = 2.0 was synthesized by the same hydrothermal method applied here, but followed by calcination at 535 °C in air, yielding a sample containing the thermodynamically stable α-MoO_3 phase, while the MoO_3 phase present directly after synthesis was h-MoO_3. In addition to the catalysts in this work, a commercial catalyst was provided by Haldor Topsøe A/S (Mo/Fe = 2.6) for reference.

Table 3 Overview of the fresh and spent catalyst characterization including XRD, Raman spectroscopy and XPS

Sample	Phases by XRD (phase wt%)	Mo/Fe bulk ratio XRD	Phases by Raman spectroscopy	Mo/Fe surface ratio XPS	XPS binding energy (eV)	
					Mo $3d_{5/2}$	Fe $2p_{3/2}$
Fresh FeMo_1.6h	h-MoO_3 (7), $Fe_2(MoO_4)_3$ (93)	1.6	h-MoO_3, $Fe_2(MoO_4)_3$	1.74	233.2	712.1
Spent FeMo_1.6h	$Fe_2(MoO_4)_3$ (85), $FeMoO_4$ (15)	1.4	$Fe_2(MoO_4)_3$	1.17	232.4	711.1
Fresh FeMo_2.0h	h-MoO_3 (18), $Fe_2(MoO_4)_3$ (82)	2.0	h-MoO_3, $Fe_2(MoO_4)_3$	3.39	233.2	712.2
Spent FeMo_2.0h	$Fe_2(MoO_4)_3$ (85), $FeMoO_4$ (15)	1.4	$Fe_2(MoO_4)_3$	1.69	232.5	711.5
Fresh FeMo_2.0α [24]	α-MoO_3 (17), $Fe_2(MoO_4)_3$ (83)	1.9	α-MoO_3, $Fe_2(MoO_4)_3$	6.09	232.0	710.8
Spent FeMo_2.0α [24]	$Fe_2(MoO_4)_3$ (69), $FeMoO_4$ (31)	1.3	$Fe_2(MoO_4)_3$, $FeMoO_4$	0.75	232.1	710.7

3.2.1 As Prepared Catalysts

As described in Sect. 2.1, the catalysts were synthesized with varying Mo/Fe ratios using a low temperature hydrothermal method. X-ray diffraction (XRD) patterns and Raman spectra (Fig. 2) of the fresh catalyst samples confirmed the presence of $Fe_2(MoO_4)_3$ indicated by the reflection at $2\theta = 25.7°$ in the XRD patterns and bands at 782, 966 and 990 cm^{-1} in the Raman spectra. Furthermore, the metastable h-MoO_3 phase was revealed by the reflection at $2\theta = 9.5°$ and bands at 250, 695 and 900 cm^{-1} in the XRD patterns and Raman spectra respectively [34]. The Mo/Fe ratio estimated from the phase composition measured by XRD of the fresh catalysts (Table 3) were similar to the ratio measured by ICP-OES (Table 1), which shows that the samples were crystalline. The presence of h-MoO_3 in the fresh catalyst samples was due to the low temperature hydrothermal synthesis method. Similar preparation of h-MoO_3 by hydrothermal synthesis have been reported in the literature [35].

The scanning electron microscopy (SEM) images (Fig. 3a, c) coupled with energy dispersive X-ray spectroscopy (EDS) showed the morphology and elemental composition of the fresh catalyst samples. FeMo_1.6h (Fig. 3a) showed the presence of agglomerates of small $Fe_2(MoO_4)_3$ crystals. FeMo_2.0h (Fig. 3c) contained similar agglomerates of $Fe_2(MoO_4)_3$ crystals and hexagonal MoO_3 crystals around 2-10 µm in size.

FeMo_2.0α, synthesized in our previous work [24], showed the presence of agglomerates of small $Fe_2(MoO_4)_3$ crystals and relatively small α-MoO_3 crystals around 1–2 µm in size (Fig. 4a, b), indicated by the reflection at $2\theta = 27.34°$ in the XRD pattern and bands at 116, 128, 665, 818 and 993 cm^{-1} in the Raman spectrum. Clear differences in the MoO_3 crystal sizes can be seen throughout samples FeMo_2.0h and FeMo_2.0α in SEM images found in Figs. S7 to S10 in the ESI.

X-ray photoelectron spectroscopy (XPS) revealed the Mo/Fe ratio from the surface region of the fresh and spent samples (Table 3). With respect to the fresh samples, it must be taken into account that they consist of both $Fe_2(MoO_4)_3$ and MoO_3, which yields a higher average Mo/Fe ratio than the one expected for solely $Fe_2(MoO_4)_3$ crystals. The XPS spectra can be seen in ESI Figs. S11 and S12. The spectra were fitted to one Mo $3d_{3/2}$–Mo $3d_{5/2}$ doublet, which indicates the presence of several types of molybdenum (VI) oxide species. The Fe $2p_{3/2}$ peak was fitted to either one or two individual components, which might indicate the presence of two iron oxide species in oxidation state II and III respectively. However, these species closely overlap, which makes quantification of the separate species highly uncertain. The Fe $2p_{3/2}$ binding energies are reported as fitted to a single Fe $2p_{3/2}$ peak. The binding energies can be seen in Table 3. Similar binding energies have been reported in the literature [36, 37].

3.2.2 Spent Catalyst

XRD patterns (Fig. 2a) confirmed that the spent catalysts were significantly depleted of MoO_3, as the reflections at $2\theta = 9.5$ and 27.3° belonging to h-MoO_3 and α-MoO_3 respectively were not observed. This depletion of Mo was expected from our previous work [24]. Likewise, SEM images (Figs. 3b, d, 4c) showed none of the initially present Mo rich crystals. $Fe_2(MoO_4)_3$ was still observed by both the XRD reflection at $2\theta = 25.7°$ and Raman spectroscopy bands as 782, 966 and 990 cm^{-1} (Fig. 2). Furthermore, $FeMoO_4$ was detected by reflections in the XRD patterns at $2\theta = 26.2°$. Detection of $FeMoO_4$ by Raman spectroscopy is difficult due to a

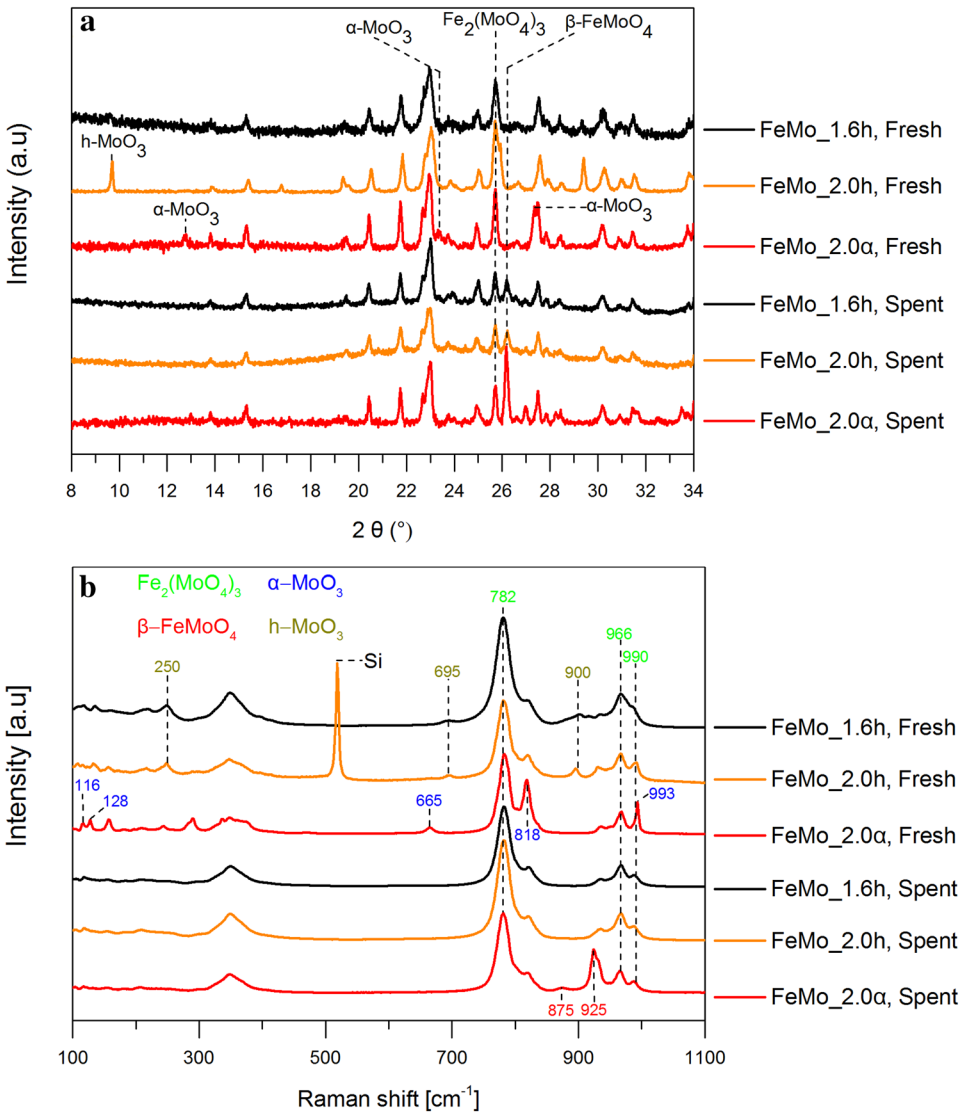

Fig. 2 **a** XRD patterns of the fresh and spent catalyst samples. **b** Raman spectra of the fresh and spent catalyst samples. A band at 518 cm^{-1} is observed for the fresh FeMo_2.0h, which is due to dilution of this sample with silicon

low Raman scattering cross section and was only clearly observed for the spent FeMo_2.0α sample (bands at 875 and 925 cm^{-1}).

XPS revealed that the surface region of FeMo_2.0α was significantly depleted for Mo. FeMo_2.0h, which had been reactivated by heat treatment, had an over-stoichiometric Mo content with Mo/Fe = 1.69 at the surface. FeMo_1.6h, which was likewise reactivated, revealed a Mo/Fe ratio of 1.17. It must be taken into account that the XPS signal originates not only from the surface, but from the top 1–2 nm of the sample. The surface monolayer thus might have a higher Mo/Fe ratio than the one measured. Nevertheless, the two catalysts heat treated after 100 h on stream showed higher Mo content in the surface region when compared to the spent FeMo_2.0α catalyst.

4 Discussion

4.1 Stability of Catalyst

For catalysts with an overstoichiometric Mo/Fe ratio, applying hydrothermal synthesis led to presence of the metastable h-MoO_3 phase for the excess molybdenum oxide (Table 3). In the case of FeMo_2.0α [24], the catalyst was calcined at 535 °C for 2 h in air as the last step of the synthesis, yielding the thermodynamically stable α-MoO_3 phase. For the two samples with a Mo/Fe ratio of 2.0, SEM images (Figs. 3c, 4b and S7 to S10 in the ESI) show the variation of their morphology. While both FeMo_2.0h and FeMo_2.0α consisted of $Fe_2(MoO_4)_3$,

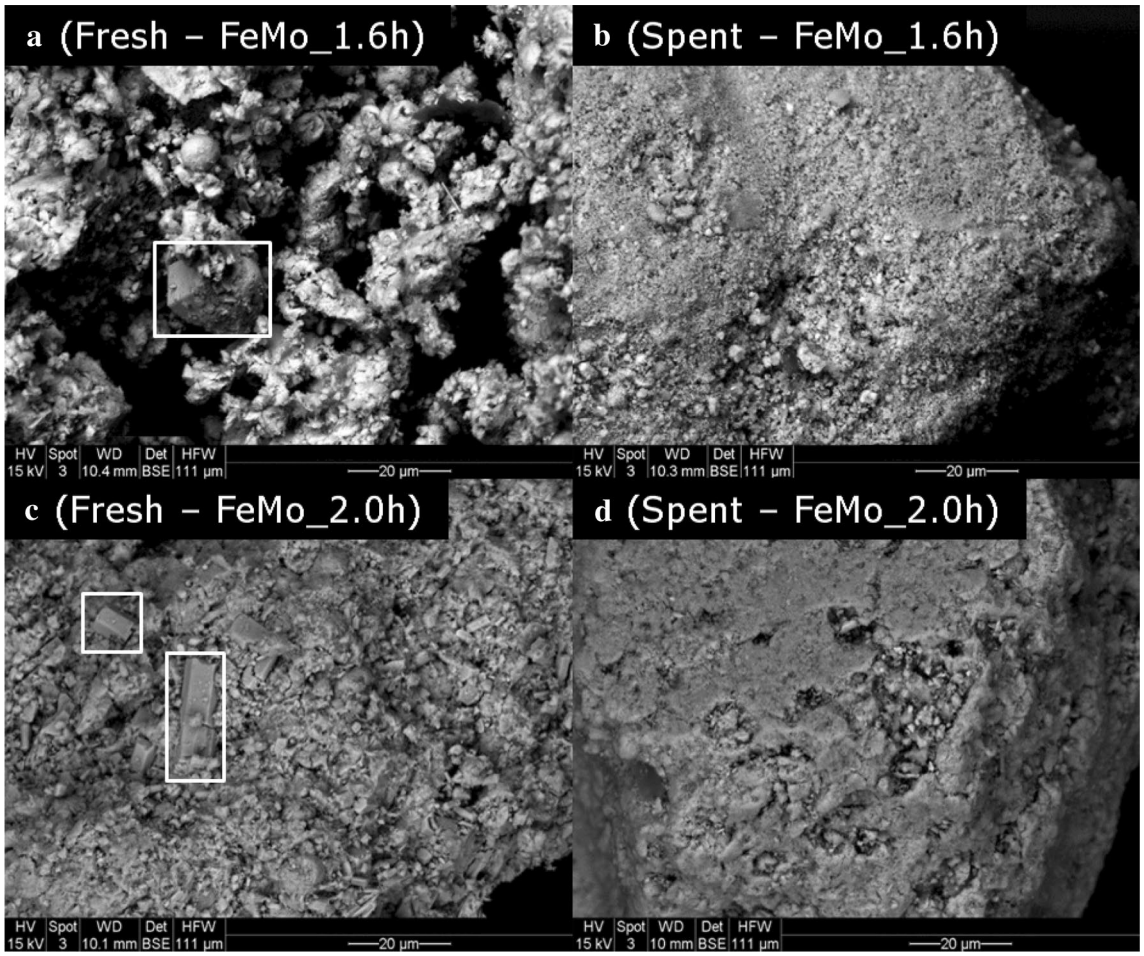

Fig. 3 SEM images of fresh and spent catalysts synthesized during this work. White rectangles mark h-MoO_3 crystals

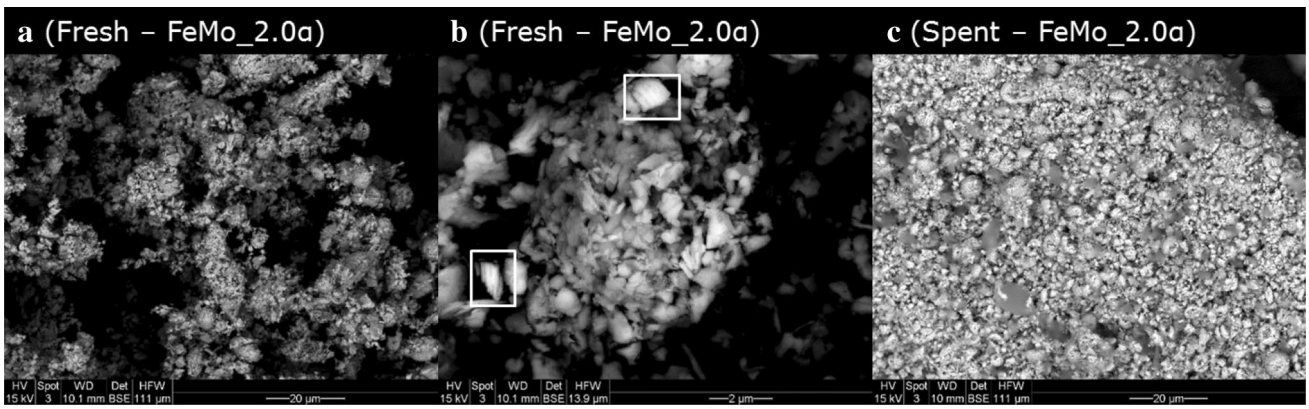

Fig. 4 SEM images of fresh and spent catalyst (FeMo_2.0α). White rectangles mark α-MoO_3 crystals. Data adapted from Raun et al. [24]

relatively large h-MoO_3 crystals (2-10 µm) were found for FeMo_2.0h and relatively small α-MoO_3 crystals (≤ 2 µm) were found for FeMo_2.0α.

The initial methanol conversion of FeMo_2.0α (48%) was significantly lower than that of FeMo_2.0h (69%). The lower activity is likely due to sintering during calcination as indicated by the SSA of the fresh samples (4.7 and 7.8 m^2/g respectively, Table 1). As discussed in the introduction (Sect. 1), the excess MoO_3 is present in the catalyst to provide high activity and selectivity and to counter the loss of

Mo from the active $Fe_2(MoO_4)_3$ phase. Although FeMo_2.0h and FeMo_2.0α possess an equal amount of MoO_3, the period for the decrease from initial to minimum activity varied significantly: 40 h for FeMo_2.0h compared to only 10 h for FeMo_2.0α. We have previously shown that the point of minimum activity corresponds to complete evaporation of all excess MoO_3 with only $Fe_2(MoO_4)_3$ left in the catalyst [24, 25]. The effect of a MeOH containing atmosphere on the MoO_3 structure was studied by *operando* Raman spectroscopy (Fig. S13). Bands related to the thermodynamically less stable h-MoO_3 at 693 and 900 cm^{-1} rapidly disappeared within 20 min on stream at 375 °C and clear bands ascribed to α-MoO_3 (284, 661 and 991 cm^{-1}) evolved simultaneously. Hu et al. [23] have shown that after calcination of h-MoO_3 in air at a proper temperature around 420-440 °C, α-MoO_3 is obtained by the process of in situ phase transformation and the morphology of the precursor (h-MoO_3) is mainly maintained. Hence, the presence of MeOH vapors lowers the temperature for rearrangement of h-MoO_3 into α-MoO_3. The rapid rearrangement of the h-MoO_3 structure into α-MoO_3 indicates that the higher stability of FeMo_2.0h compared to FeMo_2.0α cannot be ascribed to the different crystals phases, but rather to the larger MoO_3 crystals in FeMo_2.0h (Fig. 3c). Large MoO_3 crystals have a lower surface area which is likely to result in a lower rate of Mo volatilization.

Furthermore, the commercial catalyst had a Mo/Fe ratio of 2.6 and was prepared by co-precipitation followed by calcination, which yielded a catalyst containing α-MoO_3. The time for the initial decrease in activity of the commercial catalyst sample was roughly similar to the time for sample FeMo_2.0h, even though it contained a two-fold higher amount of excess MoO_3. This was likely because the commercial catalyst also contained smaller α-MoO_3 crystals, similar to FeMo_2.0α, which volatilized faster than the larger h-MoO_3 crystals in sample FeMo_2.0h. However, the higher amount of MoO_3 makes the stability of the two catalysts roughly similar. Consistent with this, the times for deactivation from initial to minimum activity for samples FeMo_1.6h and FeMo_2.0α were also similar, despite the lager amount of excess MoO_3 in FeMo_2.0α.

As discussed in the introduction, it is of high importance to obtain an active, selective and stable catalyst with a minimum amount and rate of MoO_3 volatilization to extend the operating time of the process. Preparing the iron molybdate/molybdenum oxide catalyst with large crystals and lower amounts of excess h-MoO_3 appears to be achieving exactly that.

4.2 Reactivation of Spent Catalyst

MoO_x is thermodynamically stable at the surface of the iron molybdate system [18, 38], and crystals with mainly MoO_x in the surface layer and a mixed Fe-Mo oxide phase in the sublayers have been confirmed to be highly active [14 ,39]. The observed reactivation of FeMo_1.6h, FeMo_2.0h and the commercial sample by heat treatment at 400 and 500 °C (Fig. 1) was most likely due to formation of MoO_x at the $Fe_2(MoO_4)_3$ crystal surface under simultaneous formation of $FeMoO_4$. The formed MoO_x will cover the catalyst surface, yielding a high activity. This was indicated by comparing the reactivated sample FeMo_2.0h with the non-reactivated catalyst FeMo_2.0α. The surface region of FeMo_2.0α was depleted of Mo with a Mo/Fe surface ratio of 0.75, whereas the surface Mo/Fe ratio of FeMo_2.0h was over-stoichiometric (1.69) after reactivation at 500 °C (Table 3).

5 Conclusions

In the present study iron molybdate/molybdenum oxide catalysts (Mo/Fe = 1.6, and 2.0) for selective oxidation of methanol to formaldehyde were synthesized using low temperature hydrothermal synthesis and compared to a similar catalyst (Mo/Fe = 2.0) and a commercial reference catalyst (Mo/Fe = 2.6) both calcined at high temperature. The stability of the catalysts during operation was investigated by activity measurements for 100 h (25 mg catalyst, feed flow = ~ 157.5 NmL/min, ~ 5% MeOH, 10% O_2 in N_2, temp. = 380–407 °C), and the fresh and spent catalysts were comprehensively characterized. For the hydrothermally synthesized catalysts, the excess MoO_3 was present as the metastable h-MoO_3. By calcination the thermodynamically stable α-MoO_3 formed. The commercial catalyst likewise contained α-MoO_3. All catalysts initially deactivated to a minimum activity (maximum deactivation) due to the loss of all excess MoO_3, after which they re-activated. For the catalyst with slight excess of MoO_3 (Mo/Fe = 1.6) the time for maximum deactivation was 19 h on stream. For the catalyst with Mo/Fe = 2.0 and h-MoO_3 the time to reach maximum catalyst deactivation was ~ 40 h. Comparing the two catalysts with Mo/Fe = 2.0 showed that the sample with h-MoO_3 was more stable than the sample containing α-MoO_3 (~ 40 h vs. ~ 10 h to reach lowest activity). This shows that the crystal structure, crystal size and/or morphology of the excess MoO_3 strongly affect the catalyst stability. *Operando* Raman spectroscopy showed that the initially present h-MoO_3 phase quickly rearranged to the α-MoO_3 phase. This indicates that the increased stability was mainly due to the presence of relatively large h-MoO_3 crystals (2–10 µm) compared to relatively small α-MoO_3 crystals (1–2 µm). The larger crystals of h-MoO_3 have a lower specific surface area from where volatilization of Mo can occur leading to increased stability of the catalyst.

This work shows for the first time the stabilizing effect of large hexagonal MoO_3 crystals on the iron molybdate catalyst by measuring the catalytic activity for an extended

period of time in which complete volatilization of the excess MoO_3 phase occurs. Furthermore, the possibility for reactivation of spent catalysts by heat treatment was shown. During heat treatment Mo segregated to the surface of the iron molybdate crystals in the catalyst, which improved the activity.

Acknowledgements This work is a collaboration between the CHEC research center at The Department of Chemical and Biochemical Engineering at Technical University of Denmark (DTU), Karlsruhe Institute of Technology (KIT) and Haldor Topsøe A/S. We thank the Independent Research Fund Denmark for the financial support (DFF—4184-00336).

Compliance with Ethical Standards

Conflict of Interest The authors declare that they have no conflict of interest.

References

1. Merchant Research & Consulting ltd (2016) World Formaldehyde Production to Exceed 52 Mln Tonnes in 2017
2. IHS Chemical (2013) IHS analysis report Forecast: global formaldehyde market demand after five years
3. Bahmanpour AM, Hoadley A, Tanksale A (2014) Critical review and exergy analysis of formaldehyde production processes. Rev Chem Eng. https://doi.org/10.1515/revce-2014-0022
4. Magnusson A, Thevenin P (2018) In: Informally speaking (newsletter from Formox), winter 2017/2018
5. Günther R, Disteldorf W, Gamer AO, Hilt A (2012) Ullmann's encyclopedia of industrial chemistry. Weinheim Chapter 4: Chapter 4
6. Ivanov KI, Dimitrov DY (2010) Deactivation of an industrial iron-molybdate catalyst for methanol oxidation. Catal Today 154:250–255. https://doi.org/10.1016/j.cattod.2010.03.051
7. Soares APV, Portela MF, Kiennemann A (2005) Methanol selective oxidation to formaldehyde over iron-molybdate catalysts. Catal Rev 47:125–174. https://doi.org/10.1081/CR-200049088
8. Söderhjelm E, House MP, Cruise N et al (2008) On the synergy effect in MoO_3–$Fe_2(MoO_4)_3$ catalysts for methanol oxidation to formaldehyde. Top Catal 50:145–155. https://doi.org/10.1007/s11244-008-9112-1
9. Bowker M, Carley AF, House M (2008) Contrasting the behaviour of MoO_3 and MoO_2 for the oxidation of methanol. Catal Lett 120:34–39. https://doi.org/10.1007/s10562-007-9255-x
10. Yeo BR, Pudge GJF, Bugler KG et al (2016) The surface of iron molybdate catalysts used for the selective oxidation of methanol. Surf Sci 648:163–169. https://doi.org/10.1016/j.susc.2015.11.010
11. Brookes C, Wells PP, Dimitratos N et al (2014) The nature of the molybdenum surface in iron molybdate. the active phase in selective methanol oxidation. J Phys Chem C 118:26155–26161. https://doi.org/10.1021/jp5081753
12. Bowker M, Brookes C, Carley AF et al (2013) Evolution of active catalysts for the selective oxidative dehydrogenation of methanol on Fe_2O_3 surface doped with Mo oxide. Phys Chem Chem Phys 15:11988–12003. https://doi.org/10.1039/c3cp50399b
13. Bowker M, House M, Alshehri A et al (2015) Selectivity determinants for dual function catalysts: applied to methanol selective oxidation on iron molybdate. Catal Struct React 1:95–100. https://doi.org/10.1179/2055075815Y.0000000002
14. Rellán-Piñeiro M, López N (2015) The active molybdenum oxide phase in the methanol oxidation to formaldehyde (Formox process): a DFT study. Chemsuschem 8:2231–2239. https://doi.org/10.1002/cssc.201500315
15. Popov BI, Bibin VN, Boreskov GK (1976) Study of an iron-molybfate oxide catalyst for oxidation of methanol to formaldehyde. Kinet Catal 17:322–327
16. Andersson A, Hernelind M, Augustsson O (2006) A study of the ageing and deactivation phenomena occurring during operation of an iron molybdate catalyst in formaldehyde production. Catal Today 112:40–44. https://doi.org/10.1016/j.cattod.2005.11.052
17. Pernicone N (1991) Deactivation of Fe–Mo oxide catalyst in industrial plant and simulation tests on laboratory scale. Catal Today 11:85–91. https://doi.org/10.1016/0920-5861(91)87009-C
18. Xu Q, Jia G, Zhang J et al (2008) Surface phase composition of iron molybdate catalysts studied by UV Raman spectroscopy. J Phys Chem C 112:9387–9393. https://doi.org/10.1021/jp800359p
19. Vieira Soares AP, Farinha Portela M, Kiennemann A (2005) Methanol selective oxidation to formaldehyde over iron-molybdate catalysts. Catal Rev Sci Eng 47:125–174
20. Lohbeck K, Haferkorn H, Fuhrmann W, Fedtke N (2005) Manganese and manganese alloys. Ullmann's Encycl Ind Chem. https://doi.org/10.1002/14356007.a16
21. McCarron EMI (1986) β-MoO_3: a metastable analogue of WO_3. J Chem Soc, Chem Commun 101:336–338
22. Dhage SR, Hassan MS, Yang OB (2009) Low temperature fabrication of hexagon shaped h-MoO_3 nanorods and its phase transformation. Mater Chem Phys 114:511–514. https://doi.org/10.1016/j.matchemphys.2008.10.076
23. Hu H, Deng C, Xu J et al (2015) Metastable h -MoO 3 and stable α-MoO_3 microstructures: controllable synthesis, growth mechanism and their enhanced photocatalytic activity. J Exp Nanosci 10:1336–1346. https://doi.org/10.1080/17458080.2015.1012654
24. Raun KV, Lundegaard LF, Chevallier J et al (2018) Deactivation behavior of an iron-molybdate catalyst during selective oxidation of methanol to formaldehyde. Catal Sci Technol 8:4626–4637. https://doi.org/10.1039/C8CY01109E
25. Gaur A, Schumann M, Raun KV et al (2019) Operando XAS/XRD and raman spectroscopic study of structural changes of the iron molybdate catalyst during selective oxidation of methanol. ChemCatChem. https://doi.org/10.1002/cctc.201901025
26. Beale AM, Jacques SDM, Sacaliuc-Parvalescu E et al (2009) An iron molybdate catalyst for methanol to formaldehyde conversion prepared by a hydrothermal method and its characterization. Appl Catal A Gen 363:143–152. https://doi.org/10.1016/j.apcata.2009.05.008
27. Høj M, Kessler T, Beato P et al (2014) Structure, activity and kinetics of supported molybdenum oxide and mixed molybdenum-vanadium oxide catalysts prepared by flame spray pyrolysis for propane OHD. Appl Catal A Gen 472:29–38. https://doi.org/10.1016/j.apcata.2013.11.027
28. Van Leeuwen ME (1994) Derivation of Stockmayer potential parameters. Fluid Phase Equilib 99:1–18
29. Tee LS, Gotoh S, Stewart WE (1966) Molecular parameters for normal fluids. Lennard–Jones 12–6 potential. Ind Eng Chem Fundam 5:356–363. https://doi.org/10.1021/i160019a011
30. Mourits FM, Rummens FHA (1977) A critical evaluation of Lennard–Jones and Stockmayer potential parameters and of some correlation methods. Can J Chem 55:3007–3020. https://doi.org/10.1139/v77-418
31. Coelho AA (2018) TOPAS and TOPAS-academic: an optimization program integrating computer algebra and crystallographic objects written in C++. J Appl Cryst 51:210–218
32. Braz CG, Mendes A, Rocha J et al (2019) Model of an industrial multitubular reactor for methanol to formaldehyde oxidation in

the presence of catalyst deactivation. Chem Eng Sci 195:347–355. https://doi.org/10.1016/J.CES.2018.09.033
33. Drăgan S, Kulic I (2016) A macrokinetic study of the oxidation of methanol to formaldehyde on Fe_2O_3–MoO_3 oxide catalyst. Stud Univ Babes-Bolyai, Chem, p 61
34. Lunk HJ, Hartl H, Hartl MA et al (2010) "Hexagonal molybdenum trioxide"—known for 100 years and still a fount of new discoveries. Inorg Chem 49:9400–9408. https://doi.org/10.1021/ic101103g
35. Schuh K, Kleist W, Høj M et al (2014) Selective oxidation of propylene to acrolein by hydrothermally synthesized bismuth molybdates. Appl Catal A Gen 482:145–156. https://doi.org/10.1016/j.apcata.2014.05.038
36. Bowker M, Holroyd R, House M et al (2008) The selective oxidation of methanol on iron molybdate catalysts. Top Catal 48:158–165. https://doi.org/10.1007/s11244-008-9058-3
37. Peláez R, Marín P, Ordóñez S (2016) Synthesis of formaldehyde from dimethyl ether on alumina-supported molybdenum oxide catalyst. Appl Catal A Gen 527:137–145. https://doi.org/10.1016/j.apcata.2016.09.002
38. Brookes C, Wells PP, Cibin G et al (2014) Molybdenum oxide on Fe_2O_3 core–shell catalysts: probing the nature of the structural motifs responsible for methanol oxidation catalysis. ACS Catal 4:243–250. https://doi.org/10.1021/cs400683e
39. Fagherazzi G, Pernicone N (1970) Structural study of a methanol oxidation catalyst. J Catal 16:321–325. https://doi.org/10.1016/0021-9517(70)90228-9

Affiliations

Kristian Viegaard Raun[1] · Lars Fahl Lundegaard[2] · Pablo Beato[2] · Charlotte Clausen Appel[2] · Kenneth Nielsen[3] · Max Thorhauge[2] · Max Schumann[1] · Anker Degn Jensen[1] · Jan-Dierk Grunwaldt[4] · Martin Høj[1]

[1] Department of Chemical and Biochemical Engineering, Technical University of Denmark (DTU), Søltofts Plads 229, DK-2800 Kgs. Lyngby, Denmark

[2] Haldor Topsøe A/S, Haldor Topsøes Allé 1, DK-2800 Kgs. Lyngby, Denmark

[3] Department of Physics, Technical University of Denmark (DTU), Fysikvej 311, DK-2800 Kgs. Lyngby, Denmark

[4] Institute for Chemical Technology and Polymer Chemistry, Karlsruhe Institute of Technology (KIT), Engesserstraße 20, D-76131 Karlsruhe, Germany